Organic & Biomolecular Chemistry

ROYAL SOCIETY OF CHEMISTRY

COMMUNICATION

View Article Online
View Journal | View Issue



Cite this: *Org. Biomol. Chem.*, 2023, **21**, 5762

Received 27th April 2023,
Accepted 23rd June 2023

DOI: 10.1039/d3ob00656e

rsc.li/obc



# Deoxyestrone-based lipofection agents with solution- and solid-state emission properties†

Alexander Huber,[a] Johannes Koch,[b] Kevin Rudolph,[a] Alexander Höing,[c] Fabio Rizzo,[d,e] Shirley K. Knauer[c] and Jens Voskuhl[*a]

**In this contribution, three deoxyestrone-based emissive lipofection agents are reported. Because of a centrally incorporated terephthalonitrile motif, these ligands can be classified as solution and solid-state emitters (SSSEs). With the attachment of tobramycin, these amphiphilic structures are able to form lipoplexes, mediating gene transfection of HeLa and HEK 293T cells.**

Gene delivery (or transfection) of foreign DNA or RNA into living cells plays a crucial role in the field of biomedicine because it presents a potential way of treating diseases such as Parkinson's or Alzheimer's *via* gene therapy.[1,2] However, since oligonucleotides are negatively charged under physiological conditions, the repulsive charge interactions with phospholipids of the cellular membrane prohibit membrane permeability. Therefore, several methods *e.g.* electroporation or using viral vectors have been developed.[3] Because these methods are prone to cytotoxic reactions and immunogenic effects, lipid-based ligands have been intensively studied, due to facile synthesis, low toxicity, and biodegradability in the transfection process.[4,5] The attachment of cationic headgroups for DNA binding leads to the formation of supramolecular complexes called lipoplexes, which can enter the cells *via* membrane fusion or endocytosis.[6] The importance of this process called lipofection was demonstrated by the worldwide application of mRNA vaccines against SARS-CoV-2[7] by BioNTech and Moderna.[8] The conclusive evidence of successful transfection is usually coded in the used DNA, which can express for example detectable fluorescent proteins after translation.[2]

Ligand design is crucial for an optimized lipofection process.[9] Structures of cationic lipids often feature unsaturated alkyne chains such as Felgner's *N*-[1-(2,3-dioleyloxy)propyl]-*N*,*N*,*N*-trimethylammonium chloride (DOTMA) or 1,2-dioleoyl-3-trimethylammoniumpropane (DOTAP).[10] In many reports neutral helper lipids are used, which can stabilize lipoplex formations, mediate cell fusion and enhance transfection efficiencies.[11] An example is the fusogenic lipid dioleoylphosphatidylethanolamine (DOPE), which forms Lipofectamine™ 2000 (LF 2000), the commercially available and established gold standard lipofection ligand for control experiments, together with three parts of 2,3-dioleyloxy-*N*-[2(spermine-carboxamido)ethyl]-*N*,*N*-dimethyl-1-propanaminium trifluoroacetate (DOSPA).[1] Huang's group reported that hydrophobic backbones based on steroids, such as cholesterol show elevated lipoplex stabilities and transfection efficiencies, indicating that rigidified structures can be beneficial for the transfection process.[12]

Since a versatile prediction of the transfection properties of novel amphiphiles is still challenging, a huge demand for structure–property relationship studies is required. Hence, the designs and syntheses of novel structural motifs are essential for providing insights in ligand optimization.[13]

Thus, we were interested in how subtle constitutional changes affect the morphology of self-assembled lipoplexes and their corresponding cellular uptake. Recently, we reported an estrone-based amphiphilic aminoglycoside conjugate with aggregation-induced emission (AIE) properties showing good performance in transfection experiments.[14] By taking advantages from its AIE properties, we were furthermore able to track the localisation of the transfecting ligand inside the cellular environment, which helped to gain deeper understanding of the underlying transfection process. Lipid conjugates of aminoglycosides were utilized several times in literature not

[a]*Faculty of Chemistry (Organic Chemistry), Center of Medical Biotechnology (ZMB) and Center for NanoIntegration (CENIDE), University of Duisburg-Essen, Universitätsstrasse 7, 45117 Essen, Germany. E-mail: jens.voskuhl@uni-due.de*
[b]*Center of Medical Biotechnology (ZMB), University of Duisburg Essen, Universitätsstraße 2, 45141 Essen, Germany*
[c]*Department of Molecular Biology II, Center of Medical Biotechnology (ZMB), University of Duisburg Essen, Universitätsstraße 2, 45141 Essen, Germany*
[d]*Center for Soft Nanoscience (SoN), Westfälische Wilhelms-Universität Münster, Busso-Peus-Straße 10, 48149 Münster, Germany*
[e]*Institute of Chemical Science and Technologies "G. Natta" (SCITEC), National Research Council (CNR), Via G. Fantoli 16/15, 20138 Milan, Italy*

†Electronic supplementary information (ESI) available: Synthetic procedures, transfection, toxicity, photophysical characterisation, TEM and selected spectra. See DOI: https://doi.org/10.1039/d3ob00656e

only for transfection[15,16] but also *e.g.* for detergents with antibacterial activity.[17] Therefore, in this contribution we chose the aminoglycoside tobramycin as the polar head group due to its known efficient DNA binding ability.[18] In contrast to our previous studies, we changed the AIE core system to a solution and solid-state emitter (SSSE). This phenomenon is lately popularized, since SSSEs display balanced emission when they are molecularly isolated, *e.g.* in dilute solutions, and when entrapped in closely-packed structures like aggregates or powders.[19,20] These compounds show emission independent of their state of aggregation or molecular surrounding and hence are able to overcome drawbacks such as the loss of emission in the monomeric state (AIE).[21] The design strategy of these novel transfection agents was based on our finding on bridged oxo-and thioethers featuring SSSE properties with remarkable quantum yields in solution and the solid-state.[22] Therefore, bridged ethers were merged with 17-deoxyestrone (**2**)[23] as hydrophobic tail because of its structural rigidity, similarity as well as compatibility to the cellular membrane component cholesterol. Here, we present a multistep route to three different transfecting amphiphiles (**DT**, **IT**, **IT$_2$**) with SSSE properties featuring a single tobramycin group (**T**) linked with either a dopamine (**D**) or an isoindoline (**I**) moiety (Fig. 1). In addition, an isoindoline-bearing compound connecting two DNA binding groups (**IT$_2$**) was designed to increase the hydrophilicity. In the first step the ketone group of estrone was removed *via* Wolff–Kishner reduction to enhance solubility and further increase lipophilicity, supposedly elevating interactions with the cellular membranes. To enable the monitoring of subcellular localisation, we incorporated the rigid and highly luminescent dicyanotetraoxopentacene motif as part of the lipid backbone.[24] For the etherification, the corresponding catechol **6** was synthesized *via* directed *ortho*-formylation with subsequent Baeyer–Villiger oxidation and hydrolysis (Fig. S1†). The subtle constitutional difference was integrated into the linker attaching the polar head group to the hydrophobic backbone. We synthesized first dopamine (**D**)-bearing ligand **DT**. However, we were unable to isolate **DT** regioisomerically pure and hence it was used as mixture of two isomers. Afterwards, we prepared the isoindoline (**I**) analogue **IT** by bromomethylation of veratrole (**11**) and ring-closing with *tert*-butyl carbamate (Fig. S3†). This fixed the issue of regioisomer formation elegantly, although an increased synthetic effort was necessary.

To study the effect of number of cationic charges, we synthesized ligand **IT$_2$** with two tobramycin groups using dicarboxylic acid linker **22** (Fig. S4†).[25] The three ligands **DT**, **IT** and **IT$_2$** were obtained after amide coupling of the tobramycin amine **25** [26] with the corresponding carboxylic acids **20**, **21** and **24** and BOC-deprotection with TFA, providing the corresponding TFA salts (Fig. 1 and S5†). The purity of the compounds was checked by RP-HPLC and was found sufficiently pure for our purposes (>95%, Fig. S25–S27†).

Since all compounds are expected to act as SSSEs, the photophysical properties of the compounds (Fig. S31–S34 and Table S2†) were investigated. The ligands **DT**, **IT** and **IT$_2$** show green emission ($\lambda_{em}$ around 509 nm) in dimethyl sulfoxide ($\varphi$ = 0.03 for **IT**) and as a powder ($\varphi$ = 0.17 for **IT**) with absorption maxima over 430 nm. This point is particularly important for bio-applications because the dyes can be excited with visible light, thus avoiding harmful UV irradiation. Our group previously reported the use of similar pentacene derivatives applied in bioimaging, further emphasizing the bandwidth of possible applications for these dyes.[27] Since the central terephthalonitrile moiety remains unchanged for **DT**, **IT** and **IT$_2$**, only small differences in their luminescence behaviour can be

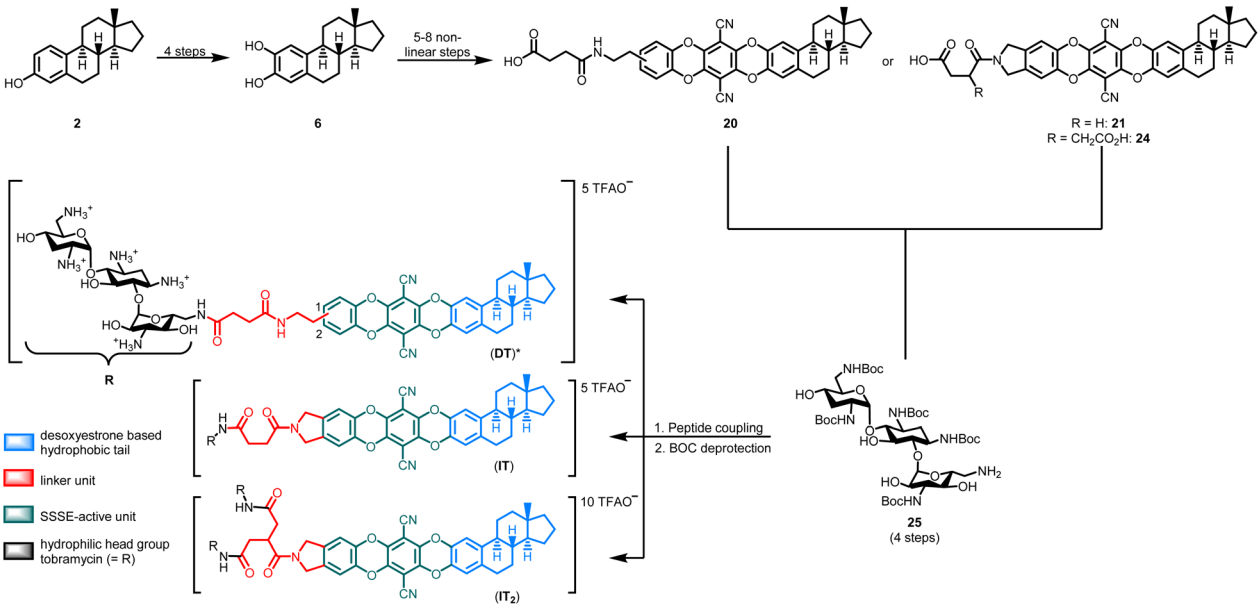


**Fig. 1** Structures and design of ligands DT, IT and IT$_2$. * The product was obtained as mixture of regioisomers on position 1 and 2.

observed. In a representative aggregation series of **IT** in tetrahydrofuran with increasing diethyl ether content, the measured emission intensity prevails in the same magnitude, demonstrating the SSSE character (Fig. 2). Interestingly, the emission quantum yield increases significantly in tetrahydrofuran ($\varphi$ = 0.56 for **IT**) with a bathochromically shifted emission wavelength compared to the DMSO solutions. By contrast, nearly no emission can be observed in water, even after the addition of pDNA (both: $\varphi$ = 0.01 for **IT**). Since the luminophores are brightly luminescent under the confocal laser scanning microscopy (CLSM) analyses (*vide infra*), we assume that the solvatochromic polarity effect and OH-vibronic coupling lead to the observed emission quenching in pure water,[28,29] similar to behaviour observed with the green fluorescent protein (GFP).[30] During the cellular uptake, the membranes encapsulate the assemblies forming endosomes, which are highly emissive due to the hydrophobic effect. To verify this hypothesis, we added surfactant Triton™ X-100 (0.5 mM) to the samples in water and observed enhanced emission (Fig. S35–S37†).

The critical micelle concentration (CMC) of Triton™ X-100 in water is 0.22 mM, thus above the CMC micelles are formed, presumably jacketing the assemblies.[31]

The ability to bind DNA was confirmed by ζ-potential measurements (Fig. S28†). All compounds are highly positive charged in aqueous media and can therefore interact with plasmid DNA (pDNA). The used pDNA in this study codes for H2B, a nuclear histone protein attached with C-terminal linked red fluorescent protein (RFP).[32]

The assemblies formed at transfection concentration conditions are highly positive (ζ-potential >20 mV), allowing the permeation of cell membranes without suffering from electrostatic repulsion.

Next, the self-assembly behaviour by transmission electron microscopy (TEM, Fig. 3 and Fig. S29, S30†) was studied. All ligands form rods with diameters of around 20 nm and lengths over 1000 nm in water. In the presence of DNA, more spherical lipoplexes can be observed. Hence, DNA is believed to be condensed inside these structures. Interestingly, the

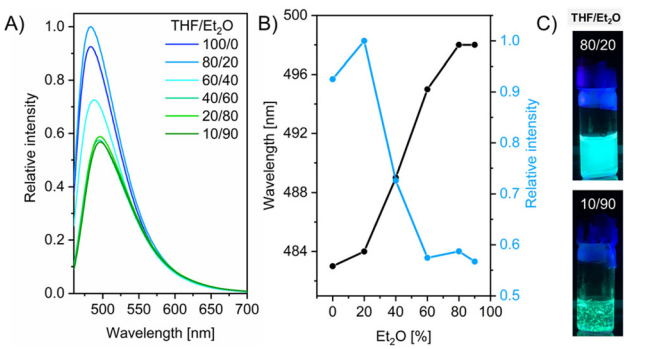


**Fig. 2** (A) Luminescence spectra of ligand **IT** in an aggregation series (10 μM in THF with increasing content of diethyl ether). (B) Corresponding emission wavelength and intensity plot. (C) Photographs of **IT** at different solvent ratios (samples irradiated at 395 nm).

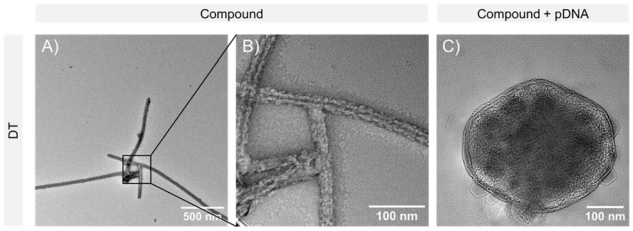


**Fig. 3** TEM images of ligand **DT** in water (A: overview; B: zoom) and in the presence of pDNA (C).

average lipoplex size varies for the three ligands (**DT**: 360 nm, **IT**: 160 nm, **IT$_2$**: 100 nm), which indicates that the structural connection and number of charges affect the morphologies of the self-assembled structures. Efforts to measure the hydrodynamic sizes *via* dynamic light scattering (DLS) failed due to inconsistent results, presumably attributable to the presence of double-lipid-layer rods which do not fulfil the spherical requirement for analysis.

With these general measurements in hand, we tested all three compounds regarding their behaviour *in vitro*. First, the cytotoxicity of the ligands was examined by MTS cell proliferation assay (Fig. 4B and S39†). Here, no significant toxicity was observed below concentrations of 50 μM, making the designed amphiphiles to ideal candidates for biomedical applications. Next, the transfection capability of the ligands using mammalian cell lines HeLa and HEK 293T and monitoring *via* CLSM was investigated (Fig. 4A and Fig. S40, S41†). We tested several concentrations and found 10 μM as the lowest concentration with good transfection efficiency. A concentration study of added pDNA revealed an optimum of 500 ng. With these optimized conditions, corresponding efficiencies were determined using CellProfiler™,[33] calculating the ratio of successfully transfected cells (segmented by RFP-H2B signal) to all cells, which were stained by CellTracker™ Deep Red[34] (Fig. 5C).

We were pleased that all ligands were able to successfully mediate gene transfection. Although the transfection efficacies are inferior compared to LF 2000™ (70% for HeLa and 50% for HEK 293T cells), this marks the first use of SSSEs in transfection combing benefits of both phenomena – aggregation induced emission (AIE) and aggregation caused quenching (ACQ). Interestingly, the use of fusogenic helper lipid DOPE present in LF 2000™ showed no improvement in the transfection efficacies for ligands **DT**, **IT** and **IT$_2$** (Fig. S42 and S43†), underlying the single-compound transfection mode of the presented amphiphiles. Regarding the relative efficiencies, **IT** exceeded for both cell lines with efficiencies above 20%. For further understanding of this trend, we studied the subcellular localisation 24 hours after treating the cells with LysoTracker™ Deep Red hoping to follow the cellular uptake mechanism. Co-localisation with a compound indicates cellular uptake *via* endocytosis followed by endosomal escape, with the compound remaining in a vesicular compartment such as a lysosome. Co-localisation was only observable for **IT$_2$** and partially for **IT**, whereas **DT** largely showed aggregate for-

 

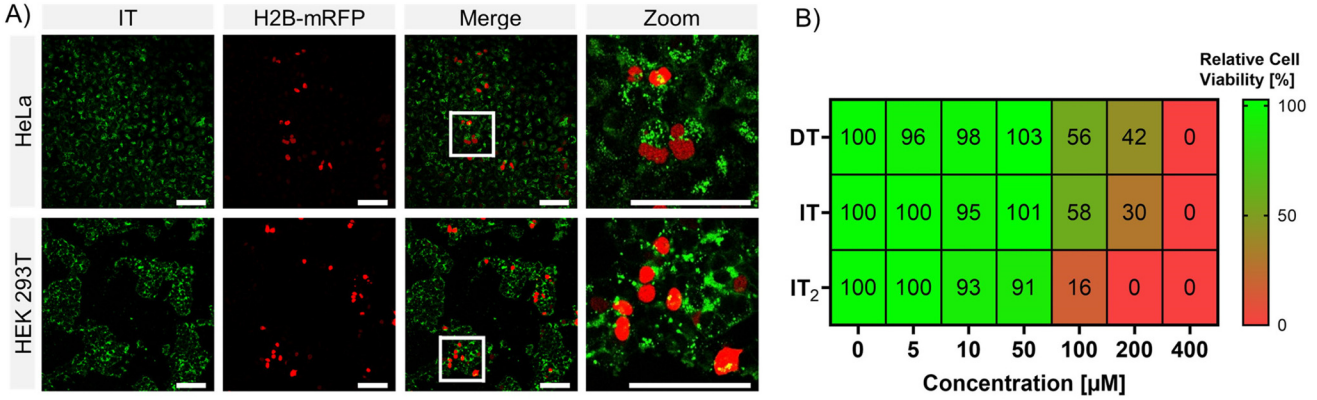


**Fig. 4** (A) Confocal laser scanning microscopy (CLSM) images of transfection experiments of ligand **IT** (10 μM, green) with mRFP-H2B (500 ng, red). Scale bar: 100 μm. (B) 24 h toxicity study investigating the effect of SSSEs on the cell viability (0.05–400 μM). For further data see ESI Fig. S39.†

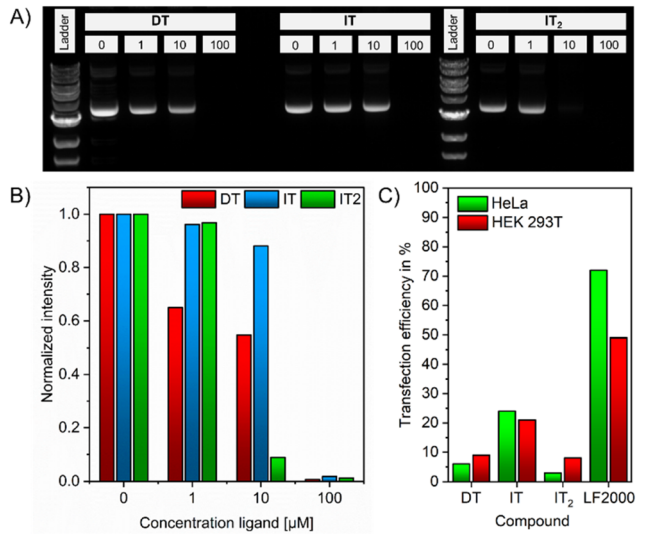


**Fig. 5** (A) Gel retardation assay (mRFP-H2B: 500 ng; ligands: 0–100 μM); (B) plotted intensity of gel retardation assay; (C) plotted transfection efficiencies.

mation (Fig. S44†). Hence, this solubility problem explains the low transfection yields of **DT** but contradicts the measured efficiency for $\mathbf{IT_2}$. Therefore, we carried out agarose gel electrophoresis with different weight ratios of the compounds (Fig. 5A, B and Fig. S45†). Upon competitive binding of a compound, the strong ethidium bromide emission resulting from intercalating DNA base pairs vanishes as lipoplexes with high retardation are formed.[35,36] This is pronounced strongly for $\mathbf{IT_2}$ with the lowest amount of free pDNA and a 10-fold emission decrease at 10 μM.

Thus, we theorize that although more hydrophilic groups enhance solubility and lipoplex formation, DNA binding becomes too effective leading to slow DNA release from the lipoplexes and low transfection efficiencies. Ligand **IT** on the other hand shows moderate tendency for DNA binding, explaining its facile release once inside the cell. In conclusion, we report the comprehensive photophysical, self-assembly and transfection investigation of the three ligands namely **DT**, **IT** and $\mathbf{IT_2}$. Small changes in the chemical configuration affect significantly the molecular geometry, photophysical properties and morphology, as determined by fluorescence, TEM and transfection experiments. Although the enhancement of the number of charges reduces the solubility problems, the subsequent very strong DNA binding causes low pDNA release. Therefore, the design of single compound lipofection agents needs modular approaches. Despite displaying low quantum yields in water, luminescence intensity rapidly increases upon changing the molecular environment to hydrophobic surroundings, allowing facile detection and characterization of the compounds *via* CLSM. The ligands **DT**, **IT** and $\mathbf{IT_2}$ are thus classifiable as SSSEs, confirming that this novel luminescence phenomenon of solution and solid-state emission can be applied to understand lipofection, further contributing to the elucidated understanding of the transfection process. In addition, these luminescent platforms can be easily modified to achieve enhanced transfection properties by balancing strong binding to DNA and efficient intracellular release utilizing cationic headgroup variations.[37,38] We believe that the SSSE phenomenon will open novel avenues for the design and application of robust imaging agents in medicine and biology in the near future.

## Author contributions

A. Huber: conceptualization, data curation, formal analysis, methodology, visualisation, investigation, writing – original draft, writing – review & editing; J. K.: data curation, formal analysis; visualisation, writing – review & editing; K. R.: data curation; A. Höing: data curation; F. R.: validation; S. K. K.: resources; J. V.: conceptualization, resources, visualization, supervision, writing – review & editing.

## Conflicts of interest

There are no conflicts to declare.

## Acknowledgements

We thank the Deutsche Forschungsgemeinschaft (DFG) – (grant: VO 2383/1-1, project number: 405679982, funding to JV, grant: RI 2635/6-1, project number: 464509280 to FR). We acknowledge the use of the imaging equipment and the support of the "Imaging Center Campus Essen" (ICCE). Instrument Leica TCS SP8X FALCON was obtained through DFG funding (Major Research Instrumentation Program as per Art. 91b GG, INST 20876/294-1 FUGG). Additionally, we thank the ICAN – Interdisciplinary Center for Analytics on the Nanoscale for providing the TEM facility.

## References

1 A. Gigante, M. Li, S. Junghänel, C. Hirschhäuser, S. Knauer and C. Schmuck, *MedChemComm*, 2019, **10**, 1692–1718.
2 M. A. Mintzer and E. E. Simanek, *Chem. Rev.*, 2009, **109**, 259–302.
3 W. S. Pear, G. P. Nolan, M. L. Scott and D. Baltimore, *Proc. Natl. Acad. Sci. U. S. A.*, 1993, **90**, 8392–8396.
4 J. P. Vigneron, N. Oudrhiri, M. Fauquet, L. Vergely, J. C. Bradley, M. Basseville, P. Lehn and J. M. Lehn, *Proc. Natl. Acad. Sci. U. S. A.*, 1996, **93**, 9682–9686.
5 H. Yin, R. L. Kanasty, A. A. Eltoukhy, A. J. Vegas, J. R. Dorkin and D. G. Anderson, *Nat. Rev. Genet.*, 2014, **15**, 541–555.
6 P. L. Felgner, T. R. Gadek, M. Holm, R. Roman, H. W. Chan, M. Wenz, J. P. Northrop, G. M. Ringold and M. Danielsen, *Proc. Natl. Acad. Sci. U. S. A.*, 1987, **84**, 7413–7417.
7 K. S. Corbett, D. K. Edwards, S. R. Leist, O. M. Abiona, S. Boyoglu-Barnum, R. A. Gillespie, S. Himansu, A. Schäfer, C. T. Ziwawo, A. T. DiPiazza, K. H. Dinnon, S. M. Elbashir, C. A. Shaw, A. Woods, E. J. Fritch, D. R. Martinez, K. W. Bock, M. Minai, B. M. Nagata, G. B. Hutchinson, K. Wu, C. Henry, K. Bahl, D. Garcia-Dominguez, L. Ma, I. Renzi, W.-P. Kong, S. D. Schmidt, L. Wang, Y. Zhang, E. Phung, L. A. Chang, R. J. Loomis, N. E. Altaras, E. Narayanan, M. Metkar, V. Presnyak, C. Liu, M. K. Louder, W. Shi, K. Leung, E. S. Yang, A. West, K. L. Gully, L. J. Stevens, N. Wang, D. Wrapp, N. A. Doria-Rose, G. Stewart-Jones, H. Bennett, G. S. Alvarado, M. C. Nason, T. J. Ruckwardt, J. S. McLellan, M. R. Denison, J. D. Chappell, I. N. Moore, K. M. Morabito, J. R. Mascola, R. S. Baric, A. Carfi and B. S. Graham, *Nature*, 2020, **586**, 567–571.
8 J. Kim, Y. Eygeris, M. Gupta and G. Sahay, *Adv. Drug Delivery Rev.*, 2021, **170**, 83–112.
9 J. Buck, P. Grossen, P. R. Cullis, J. Huwyler and D. Witzigmann, *ACS Nano*, 2019, **13**, 3754–3782.
10 P. L. Felgner and G. M. Ringold, *Nature*, 1989, **337**, 387–388.
11 Z. Du, M. M. Munye, A. D. Tagalakis, M. D. I. Manunta and S. L. Hart, *Sci. Rep.*, 2014, **4**, 7107.
12 S. Li, X. Gao, K. Son, F. Sorgi, H. Hofland and L. Huang, *J. Controlled Release*, 1996, **39**, 373–381.
13 S. Riebe, A. Zimmermann, J. Koch, C. Vallet, S. K. Knauer, A. Sowa, C. Wölper and J. Voskuhl, *RSC Adv.*, 2020, **10**, 19643–19647.
14 A. Zimmermann, Q. Z. Jaber, J. Koch, S. Riebe, C. Vallet, K. Loza, M. Hayduk, K. B. Steinbuch, S. K. Knauer, M. Fridman and J. Voskuhl, *ChemBioChem*, 2021, **22**, 1563–1567.
15 J. Hu, L. Yang, X. Cheng, Y. Li and Y. Cheng, *Adv. Funct. Mater.*, 2021, **31**, 2103718.
16 M. C. Bellucci and A. Volonterio, *Antibiotics*, 2020, **9**, 504.
17 S. Bera, G. G. Zhanel and F. Schweizer, *J. Med. Chem.*, 2008, **51**, 6160–6164.
18 P. Belmont, A. Aissaoui, M. Hauchecorne, N. Oudrhiri, L. Petit, J.-P. Vigneron, J.-M. Lehn and P. Lehn, *J. Gene Med.*, 2002, **4**, 517–526.
19 A. Huber, J. Dubbert, T. D. Scherz and J. Voskuhl, *Chem. – Eur. J.*, 2023, **29**, e202202481.
20 J. L. Belmonte-Vázquez, Y. A. Amador-Sánchez, L. A. Rodríguez-Cortés and B. Rodríguez-Molina, *Chem. Mater.*, 2021, **33**, 7160–7184.
21 G. Chen, W. Li, T. Zhou, Q. Peng, D. Zhai, H. Li, W. Z. Yuan, Y. Zhang and B. Z. Tang, *Adv. Mater.*, 2015, **27**, 4496–4501.
22 S. Riebe, S. Adam, B. Roy, I. Maisuls, C. G. Daniliuc, J. Dubbert, C. A. Strassert, I. Schapiro and J. Voskuhl, *Chem. – Asian J.*, 2021, **16**, 2307–2313.
23 M. I. Quindt, G. F. Gola, J. A. Ramirez and S. M. Bonesi, *J. Org. Chem.*, 2019, **84**, 7051–7065.
24 J. Dubbert, M. Valtolina, A. Huber, T. D. Scherz, C. Wölper, C. G. Daniliuc, O. Filiba, S. Sen, I. Schapiro, F. Rizzo and J. Voskuhl, *ChemPhotoChem*, 2023, **7**, e202200169.
25 L. de Jong, E. A. de Koning, W. Roseboom, H. Buncherd, M. J. Wanner, I. Dapic, P. J. Jansen, J. H. van Maarseveen, G. L. Corthals, P. J. Lewis, L. W. Hamoen and C. G. de Koster, *J. Proteome Res.*, 2017, **16**, 2457–2471.
26 I. M. Herzog, M. Feldman, A. Eldar-Boock, R. Satchi-Fainaro and M. Fridman, *MedChemComm*, 2013, **4**, 120–124.
27 J. Dubbert, A. Höing, N. Graupner, Ľ. Rajter, M. Dunthorn, S. K. Knauer, A. Galstyan, F. Rizzo and J. Voskuhl, *Chem. – Eur. J.*, 2023, e202300334.
28 J. Maillard, K. Klehs, C. Rumble, E. Vauthey, M. Heilemann and A. Fürstenberg, *Chem. Sci.*, 2021, **12**, 1352–1362.
29 G. E. Dobretsov, T. I. Syrejschikova and N. V. Smolina, *Biophysics*, 2014, **59**, 183–188.
30 G.-J. Huang, J.-H. Ho, Ch. Prabhakar, Y.-H. Liu, S.-M. Peng and J.-S. Yang, *Org. Lett.*, 2012, **14**, 5034–5037.
31 G. E. Tiller, T. J. Mueller, M. E. Dockter and W. G. Struve, *Anal. Biochem.*, 1984, **141**, 262–266.
32 R. E. Campbell, O. Tour, A. E. Palmer, P. A. Steinbach, G. S. Baird, D. A. Zacharias and R. Y. Tsien, *Proc. Natl. Acad. Sci. U. S. A.*, 2002, **99**, 7877–7882.
33 D. R. Stirling, M. J. Swain-Bowden, A. M. Lucas, A. E. Carpenter, B. A. Cimini and A. Goodman, *BMC Bioinf.*, 2021, **22**, 433.

 

34 W. Zhou, H. C. Kang, M. O'Grady, K. M. Chambers, B. Dubbels, P. Melquist and K. R. Gee, *J. Biol. Methods*, 2016, **3**, e38.
35 B. Wang, P. Chen, J. Zhang, X.-C. Chen, Y.-H. Liu, Z. Huang, Q.-Y. Yu, J.-H. Zhang, W. Zhang, X. Wei and X.-Q. Yu, *Polym. Chem.*, 2017, **8**, 7486–7498.
36 B. Wang, J. Zhang, Y.-H. Liu, W. Zhang, Y.-P. Xiao, R.-M. Zhao and X.-Q. Yu, *J. Mater. Chem. B*, 2018, **6**, 2860–2868.
37 S. Junghänel, S. Karczewski, S. Bäcker, S. K. Knauer and C. Schmuck, *ChemBioChem*, 2017, **18**, 2268–2279.
38 W. Liang and J. K. W. Lam, in *Molecular Regulation of Endocytosis*, ed. B. Ceresa, InTech, 2012.